RSC Advances

PAPER

View Article Online
View Journal | View Issue

Cite this: *RSC Adv.*, 2017, **7**, 43600

Understanding the wear behaviour of non-doped and Si,O-doped diamond-like carbon films

Joseph Lanigan,*[a] Helen M. Freeman,[ab] Chun Wang,[a] Michael B. Ward,[c] Ardian Morina,[a] Anne Neville[a] and Rik Brydson[c]

Received 13th August 2017
Accepted 5th September 2017

DOI: 10.1039/c7ra08959g

rsc.li/rsc-advances

Two diamond-like carbon coatings have been examined, both prior to, and post tribotesting. Physical–chemical characterisation allows the elucidation of both the physical and tribochemical mechanisms underpinning the respective wear behaviours. The wear of the undoped a-C:H DLC coating is far lower than that of the Si,O-doped DLC. Both coatings show formation of protective tribofilms with tribochemically-relevant elements derived from the lubricant additives; however the tribofilms on the two coatings exhibit key differences, with one containing pyrophosphate. The undoped a-C:H DLC coating shows an increase in non-planar sp^2 carbon content during wear testing which appears to be at the expense of sp^3-hybridised carbon. In comparison, the Si,O-doped DLC undergoes comparatively little change in carbon hybridisation state.

Introduction

DLC coatings are designed to be inherently low wearing materials. Like many carbonaceous materials, they are able to undergo changes in carbon hybridisation state, or "re-hybridise" (*i.e.* transform from carbon sp^3 to sp^2 bonds). One prominent example of this is the change in $sp^2 : sp^3$ ratio that can occur upon high-temperature heating of DLC coatings.[1–4] DLC coatings with high sp^3 fractions are frequently regarded as intrinsically low wearing, due to their high hardness.[5]

Literature on tribologically induced changes of hybridisation of DLCs is somewhat lacking. Furthermore, the phenomena are complicated by accurate characterisation of carbon $sp^2 : sp^3$ ratios. Most often, due to ease of use, the technique employed to detect changes in carbon hybridisation state within the film is Raman spectroscopy.[2,6] However, Raman spectroscopy is known to have limitations when examining DLC films. These include an uncertainty in the beam penetration depth, and appropriate selection of excitation wavelength, which means that the technique may not assess the film accurately.[7,8] DLC films are usually 1–3 μm thick and carbon bonding within the film is known to change with depth. Interlayers used to improve the DLC–metal bonding frequently form carbides and are not representative of the film, particularly for the top layer which is crucial to friction and wear performance. As such, Raman analysis was not conducted here. Fortunately, there are a variety of other spectral techniques which can be used to establish sp^2 content in DLC films; Electron Energy Loss Spectroscopy (EELS) and Nuclear Magnetic Resonance (NMR).[9,10] These two techniques were used in this study and are discussed later.

Due to its inability to form stable double bonds, Si doping is often employed to enhance the sp^3 content of DLC coatings[11] which is frequently regarded as a beneficial characteristic[12] and is known to positively affect many attributes of DLC coatings. These include: decreasing the dry-friction coefficient, increasing the coating adhesion to the metal substrate and altering the water wettability of the coating.[13–17] Conversely, when in oil lubricated conditions, doping with Si appears to be associated with certain negative aspects such as increased wear rates and the loss of enhanced-lubricity.[13,14,16,18,19]

The wear behaviour of DLC coatings is generally maintained when under oil lubrication and can be enhanced by certain oil additives, including Zn DialkylDithioPhosphates (ZDDP).[20] Examples of additives causing higher wear of DLC coatings have been noted; specifically the friction-reducing molybdenum species.[21] The behaviour and performance of ZDDP in base oil at steel/steel contacts is very well understood. In brief, the anti-wear (AW) performance of ZDDP is closely related to the ability of ZDDP to form zinc polyphosphate glasses.[22] Recently, molecular dynamics simulations of ZDDP tribofilms on steel have helped highlight the molecular origin of how antiwear films are able to form, function, and also dissipate energy.[23] It has been established that the anti-wear effects of the ZDDP-derived tribofilms originate from changes caused by the contact pressure on the coordination number of the atoms acting as cross-linking agents, enabling the formation of chemically connected networks.[23]

[a]*Institute of Functional Surfaces, School of Mechanical Engineering, University of Leeds, Leeds, LS2 9JT, UK. E-mail: j.lanigan@leeds.ac.uk*

[b]*Helmholtz Research Centre, GeoForschungsZentrum, Telegrafenberg, 14473 Potsdam, Germany*

[c]*Institute for Materials Research, School of Chemical and Process Engineering, University of Leeds, Leeds, LS2 9JT, UK*

In a fully-formulated lubricant, ZDDP is typically included with a variety of other species, including Ca based detergents, friction modifiers, dispersants and viscosity modifiers. This complex lubricant formulation is required for effective lubrication within the internal combustion engine. However, the interaction between many of these additives is not always beneficial. The dithiophosphate ligand in ZDDP has well known cation binding affinities which include many metals regularly encountered within an engine. The effect of the replacement of Zn with different metal cations contained in the full additive package is variable, and depends on the newly introduced cation, and the type of film formed. Organic species in lubricant packages are also known to hinder the performance of ZDDP, such as amine-containing additives.[24] It has been established that incorporation of Ca with ZDDP in a lubricant package results in the formation of a chemically different tribofilm on ferrous surfaces, where Ca competes with the Zn cation for reaction with the phosphorous source.[25] Long chain polyphosphates are not formed,[26,27] but instead, the formation of Ca phosphates are frequently noted within the worn area.[25,27] It is also known that combining Ca species within a ZDDP-containing additive package, when tested on steel, results in a decrease in the anti-wear effectiveness as compared to ZDDP alone.

This current work aims to investigate the wear of boundary-lubricated DLC/steel contacts, with ZDDP in the formulated lubricant, for the case of two very different DLC coatings: an undoped a-C:H DLC coating and a Si,O-doped DLC coating. It uses a range of analytical techniques to investigate the tribofilm formation and quantify any change in carbon hybridisation state within the DLC coating itself to then relate this to the measured wear performance.

Materials and methods

Diamond-like carbon coatings

The two coatings examined were both hydrogenated DLC coatings. The DLCs were produced by Sulzer Sorevi and are known under the trade name 'Dylyn'. The Si doped coating is also from this famil and includes an organometallic precursor that provides the source of Si and O. The manufacturer's parameters stated that the thickness of the films (prior to testing) were 2.4 μm for the Si,O-DLC and 1.4 μm for the a-C:H DLC. The Si-doped coating also included a significant amount of O, due to the organometallic precursor material employed for doping (the composition of which is commercially sensitive and therefore not given). The results from Elastic Recoil Detection Analysis (ERDA) of both coatings are given in Table 1. The DLC coatings were deposited on AISI 52100 steel plates of dimensions 7 × 7 × 3 mm with a maximum roughness of (R_a) 80 nm.

The coatings were produced using low temperature plasma, the exact deposition parameters were not given, as they are commercially sensitive. The substrate was negatively biased by 500 V with the chamber acting as the electrode. A hot cathode auxiliary system was also employed to enhance plasma generation. The process typically takes place at 10^{-3} mbar. The substrate was first cleaned by Ar ion etching before deposition, and then a Ti layer was deposited, followed by a Si based interlayer to improve coating adhesion to the substrate. After interlayer deposition the bulk DLC was deposited. Table 1 details the coating's properties.

Table 1 Gives ERDA data from the coating's manufacturer. It is noted that this technique is not specifically surface sensitive. As such, the 0% oxygen value for a-C:H could be as high as the atom accuracy value, given in the table. Prior to testing, the samples were stored in a sealed, protected environment. This is a commercial packaging technique used to prevent oxidation

	Element%				
Coating	C	H	O	Si	Ar
a-C:H	67	34	0	n/a	0.2
Si,O-DLC	56	34	7	14	0.4
Atom accuracy±	3	2	2	2	0.05

Tribometer testing procedure

Both DLC coatings were paired with a non-coated steel counter body. The counter body was an AISI 52100 steel pin with a semi-spherical end and a radius of 120–150 mm, with a Rockwell hardness value of 58–60 HRC, the C denoting the type of indenter used. The pins had a maximum roughness (R_a) of 0.3 μm. Testing conditions, shown in Table 2, were chosen to simulate the lower pressure internal combustion engine piston-ring/liner type contact. This is where high levels of wear are found in engines and where DLCs are being to combat this. In this case boundary lubrication was confirmed by the lambda ratio value (λ) for the initial system setup which was calculated as being 0.0040.

The Cameron-Plint 'TE77' reciprocating pin-on-plate tribometer allows for tribological investigations under different temperatures and loads. Before experimental set-up all parts were sonically cleaned in acetone for twenty minutes. Heating was controlled by a thermo-couple that regulates the oil temperature according to a user defined value (in this case 100 °C). This temperature was chosen to match the temperature of a working car engine. The heater plate is positioned below the sample holder. The load cell can measure the frictional force and converts this to a digital signal, using an analogue to digital converter. This is then processed by LabVIEW. The frictional

Table 2 Tribometer running conditions

Running conditions	Piston ring conditions
Load	28 N
Maximum Hertzian pressure	0.15 GPa
Lambda ratio (λ)	0.004
Running speed	0.2 m s^{-1}
Temperature	100 °C
Frequency	20 Hz
Volume of oil	4 ml
Pin radius	120–150 mm
Test duration	7 and 14 hours

force is the average of 1000 measurements read at five minute intervals. Once finished, the pin and plate were rinsed in heptane to remove excess oil and stored in aluminium foil to avoid contamination. The experimental parameters are detailed below in Table 2.

Lubricant

The lubricant used in this study was a fully-formulated, commercially-available diesel engine oil. The oil manufacturer was Lubrizol Ltd. The viscosity of the lubricant at 100 °C was 12.31 cSt. As a commercial sample, its exact composition was not disclosed. The oil was of 10w40 viscosity grade and meets Euro 6 standards. ICP analysis was provided for the oil. This data confirmed the oil contain Ca, P, S and Zn. ppm values from ICP confirm that the elements were blended in at the following concentrations (in ppm): Ca 2391, Mg 81, P 761, S 2064, and Zn 833. Zn is present as ZDDP blended into the lubricant. The oil also contains anti-oxidants, detergents and dispersants and the friction modifier (1.5% w/v) species: Glycerol Mono-Oleate (GMO).

Analytical methods

Nanohardness

Surface hardness values were obtained using a Nanotest™ Nano indenter produced by Micro Materials Ltd Wrexham, UK. The test apparatus is in an enclosed, temperature regulated box to ensure no fluctuations due to heating or cooling processes. The Nanotest platform software suite and micro capture camera were used to obtain, analyse and interpret the data. Following the experimental method devised by Oliver and Pharr,[28] a diamond-tipped probe with a Berkovich indenter of 130° was employed for testing. All samples were mounted to the holder using a high strength adhesive. The maximum penetration depth employed was 51 nm, as the average roughness of the film was much greater, recorded as 41 μm. One hundred measurements were made both within and outside of the worn area and a standard deviation of the data calculated.

Non-contact profilometry

Post wear surface analysis was conducted to fully characterise volume loss of the coating and to work out dimensional wear coefficients. Scanning white light interferometry was conducted on a Bruker NP FLEX™ interferometer which moves in 3-dimensions to produce an image of the surface examined. The 'Vision64' software suite is then used to analyse the data obtained and remove surface bias such as curvature and tilt giving information on the volume of material lost and surface roughness.[29] All measurements were taken using the vertical scanning interferometry (VSI) mode with a magnification of ×2.5.

X-ray photoelectron spectroscopy (XPS)

XPS was employed to assess the chemistry of any tribofilms formed due to tribochemical interactions that may have occurred at the surface. XPS was carried out using a VG ESCALAB 250 X-ray Photoelectron Spectrometer using monochromatized X-rays from an aluminium K-alpha source. An approximate area of 500 μm^2 was analysed in the wear scar.

XPS is surface specific in that it can only penetrate the upper few nanometres (typically 5–10 nm) of the sample.[30] Initially a short survey scan was carried out to determine which elements were present. This was done with the settings of 200 eV pass energy, 1 eV energy step size and a 50 ms dwell time. Longer (high resolution) scans of selected photoelectron peaks were carried out to identify specific (chemical) components present. The settings for the high-resolution scans were: 40 eV pass energy, 0.1 eV energy step size and 100 ms dwell time. CASA XPS software was used to analyse the data. Reported literature C 1s calibration data for various DLC and Si,O-DLC samples were in agreement with the calibration reference value of 284.4 eV for the main C–C peak component.[6,31–33] Evaluation of the Si 2p peak position was also verified using literature values.[6,34,35]

Focused ion beam (FIB)

A FEI Nova200 Nanolab dual beam Focused Ion Beam/Scanning Electron Microscope (FIB/SEM) was used to create thin, site-specific cross sectional lamellae from the worn area for examination by Transmission Electron Microscopy (TEM). To protect the area of interest from the ion beam, an initial 1.5 μm thick layer of platinum was deposited as a strip on top of the worn area using a gas injector and the electron beam. Once this was complete, material either side of the deposited Pt layer was milled away to an approximate depth of 10 μm below the surface using a 30 kV gallium ion beam. The cross section was thinned further and then cut away from the bulk material. The sample was then attached to a copper TEM grid using a micromanipulator; attachment being achieved by bonding with Pt. The thin lamella was given a final ion beam polish using a lower ion beam energy and current.

Transmission electron microscopy (TEM)

A Philips/FEI CM200 FEGTEM Field emission gun TEM/STEM operated at 200 kV and equipped with a Supertwin Objective lens, cryoshielding, an Oxford Instruments INCA EDX system and a Gatan Electron Energy Loss Spectrometer (EELS) (Gatan Imaging Filter GIF 200) was used to image and analyse any tribolayers present, as well as investigate the coating microstructure. The FIB sample preparation and TEM examination can cause sample damage. A protective Pt strap was used in the FIB to minimise ion implantation and sample damage, although this is known to still occur at the surfaces of the thin TEM lamella. Damage by both ions and electrons occurs by both knock-on (and hence surface sputtering and mass loss) and also radiolysis.[36,37]

For hydrogenated carbon materials, one of the main concerns is removal of hydrogen, present as C–H bonds, and also potentially by release of interstitial hydrogen gas.[38,39] Ideally, one would use low fluence (electrons per nm^2) conditions, below the sputtering threshold energy for the particular element in question. For carbon this is approximately 80 keV, however for hydrogen this will be very much lower. For TEM

imaging at 200 kV this is not a major issue due to the relatively short image acquisition times and subsequent low electron fluences. However for the longer acquisition times required for EELS analysis this can be more of an issue.[40] To avoid significant levels of electron irradiation induced damage, TEM images were focused away from the region of interest; the sample area was then moved into the beam and data was captured promptly. The dose rate for these experiments was of the order 10^4 electrons per nm^2 per s. This procedure is in-line with literature standards, known to reduce electron beam damage of samples.[41] There have been a number of studies conducted on DLC films using TEM and EELS in order to extract the carbon sp^x ratios. These include LiBassi *et al.*,[42] Shindo *et al.*[43] and Ponsonnet *et al.*;[10] the latter two publications provide somewhat conflicting reports of the importance of damage.

Electron energy loss spectra (EELS)

EELS spectra were recorded using a Gatan Imaging Filter and initially processed using the Gatan Digital Micrograph software suite. EELS carbon K-edge spectra were analysed to investigate the carbon hybridisation state in the worn area as a function of wear. Analysis was achieved using Gaussian peak fitting in HyperSpy[40] to quantify the ratio of non-planar sp^2 to planar sp^2 carbon bonding. A detailed discussion of this analysis procedure can be found in,[40] but in brief, five Gaussian peaks (G1 to G5) are fitted to the spectrum, an example of which is shown in Fig. 3. The relative area under the first Gaussian peak centred at 285 eV, over the π^* peak (labelled G1), provides information about the proportion of carbon atoms which are planar sp^2-bonded, whilst the sum of the areas under the second and third Gaussians, labelled G2 and G3, provides information about the proportion of non-planar, carbon sp^2-bonding, similar to that found in fullerenes. These areas are both normalised to the total carbon K-edge intensity (integrating over a 20 eV window from the edge onset at 282.5 eV). To calculate the % planar sp^2-bonding the extracted data is normalised to a reference material. In this case, this is a highly ordered graphite used in the nuclear industry (Pile Grade A), assumed to have 100% planar sp^2 bonding. However, to calculate the relative amount of non-planar sp^2 carbon atoms the normalised contribution of the G2 and G3 peaks in the (100% planar sp^2 carbon) reference material must first be subtracted from the sum of the G2 and G3 peaks in the fitted spectrum. In a pure carbon material, this allows for the fraction of non-planar sp^2 carbon to planar sp^2 carbon atoms to be determined.

It is noted that, in addition to carbon, the presence of heteroatoms may add intensity in the region covered by Gaussians G2 and G3.[40] C–H bonds are reportedly observed in DLC films at energy positions around 287.5 eV, which would contribute to this calculated G2 + G3 intensity.[10] However, the hydrogen content of the two films studied are equal (Table 1) and, as discussed previously, at 200 kV and room temperature it is expected that hydrogen will be removed from the thin TEM lamella by knock on damage. Furthermore, the presence of Si and O in Si,O-doped DLC may also result in C–Si and C–O bonds which could contribute to the intensity in this region. This point is explored in more depth later.

Solid-state magic angle spinning NMR

Solid state magic angle spinning NMR was used to analyse the DLC films and further validate carbon sp^x ratios. NMR is a very useful technique for probing carbon chemical state environments; however it is not surface sensitive and instead examines the bulk of a material. NMR works by interacting with non-spin paired nuclei, in the case of carbon the isotope that is most abundant is not NMR active. However ^{13}C is NMR active and as this isotope represents approximately 1% of all total carbon atoms, a sample of sufficient mass needs to be prepared. NMR probes the spin environment of relevant nuclei and returns chemical shift values of the different species. This is immensely useful for DLCs as carbon NMR chemical shift values can be used to establish the $sp^3 : sp^2$ ratio of carbon atoms in a sample.[9]

Solid-state ^{13}C spectra were recorded at 100.56 MHz using a Varian VNMRS spectrometer and a 6 mm (rotor outer diameter) magic-angle spinning (MAS) probe. They were obtained using cross-polarisation with TOSS spinning sideband suppression with a 1 s recycle delay, 1 ms contact time, at ambient probe temperature (~25 °C) and at a sample spin-rate of 6.8 kHz. 3712 and 56 128 repetitions were accumulated for the a-C:H DLC and Si,O-DLC, respectively. Spectral referencing was with respect to an external sample of neat tetramethylsilane (carried out by setting the high-frequency signal from adamantane to 38.5 ppm). For this investigation, cross-polarisation was used, a technique that transfers radio frequency energy from hydrogen nuclei to carbon nuclei. This is useful for two reasons: firstly it has been previously detailed in the literature[9] on DLC and secondly, it increases the response from the carbon nuclei and focuses the spectral data to carbons directly bonded to hydrogen atoms.

The Si,O-doped and a-C:H DLC samples were converted to powder, prior to any tribological testing, to allow for NMR analysis. The powders were prepared using a modified literature procedure.[9] A large coated aluminium substrate (~200 cm^2 and 10 μm thick) was soaked in 15% hydrochloric acid solution for two hours with external cooling. The DLC material remained intact. The metal substrate, including the interlayers, were sequestered by the acid resulting in black, flake-like product that was filtered from the solution, washed with purified water and heptane and then finally dried at 40 °C overnight. Between 50–100 mg (50 mg a-C:H, 100 mg Si,O-doped) of the DLC powders from each sample were obtained and sent for ^{13}C MASNMR analysis. A greater amount of the Si,O-DLC was required in order to obtain sufficient signal from the sample, as incorporation of Si correlates with a decrease in carbon content of the overall coating.

A typical NMR spectrum of DLC is composed of a few broad peaks, depending on the doping elements contained and their % atomic levels. Specifically when doping with Si,O precursors there is potential for additional oxygenated species to occur.[9] Typically the C sp^2 peak appears at around 125–130 ppm and the C sp^3 peak appears at around 20–35 ppm. These values may shift depending on, in the case of DLC, incorporation of O or Si. Solid-state MASNMR data is shown without repeats due to the

difficulty in synthesis of the large amount of DLC material required. As such the MASNMR data was used to confirm the known trend that Si incorporation increases the amount of C–C bonding.[44]

Results

Pre-wear solid-state NMR analysis

Pre-wear solid-state ^{13}C MASNMR data is shown in Table 3. The Si,O-DLC has a greater ratio of sp^3 bonded carbons when compared to the a-C:H film, as expected since Si does not readily take part in sp^2 bonding with carbon.[45]

Friction performance of the DLC coatings

The friction values obtained for both the coatings over a 14 hour period are presented in Fig. 1 and Table 4. Neither the full friction trace nor the steady state values show much difference in the performance of the two coatings. These results are in-line with literature precedents of Si,O-DLCs tested in formulated oil, in that the inherently improved lubricity when compared to other DLCs, is lost when tested in fully-formulated lubricants.[18,19,46]

Table 3 Pre-wear ^{13}C solid state MASNMR data of both coatings, nd = not detected

NMR peak assignments	a-C:H (%)	Si,O-DLC (%)
sp^3	38.2	53.1
sp^2	55.1	46.9
C–O type	6.7	nd

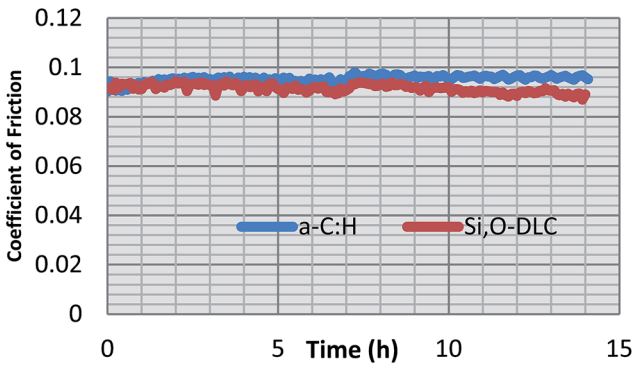

Fig. 1 Friction profile of both DLCs tested.

Table 4 Steady state friction and final wear values. Experimental deviation values are standard deviation from three repeat experiments

Coating	Steady state friction	Specific wear rate, ($k \times 10^{-18}$ m^3 Nm^{-1})
a-C:H	0.10 ± 0.002	2.8 ± 0.2
Si,O-DLC	0.09 ± 0.003	4.5 ± 0.2

Wear

Wear analysis was undertaken at the end of testing of the DLC-coated plates. Worn volumes were converted into dimensional wear coefficients, shown in Table 4, which allows for comparisons to be made with similar coatings/materials. It must be noted that despite Si,O-DLC having a higher wear rate than the a-C:H DLC, both DLC coatings appear to experience only polishing wear. For both DLCs the coating was intact at the end of the testing period.

Nanohardness values

Nanohardness data of the unworn and worn coatings is presented in Table 5. 100 indentations were averaged to obtain these values. For both coatings, there is no change within standard deviation between the unworn and worn values.

XPS results

XPS data, shown in Table 6, confirms the presence of a tribofilm on both the DLC coatings. Notable elements include Ca, S and Zn in both films. Interestingly, no P is detected in the worn area of the a-C:H film, whereas P is present as pyrophosphate (calcium phosphate, in this instance) in the wear track of the Si,O-DLC.[47] The presence of P is noteworthy as certain pyrophosphate (PO_3^-) species are known to be relevant in terms of anti-wear films on ferrous materials.[22] Various sources of O are available to both coatings, as the lubricant contains over-based $CaCO_3$ as well other oxygenated additives. Therefore, it does not seem to be the case that O from either coating is sequestered to produce the pyrophosphate groups observed. The tribofilm formed is distinct from a thermal film, as the elements within the worn area are present in far higher concentrations than outside of the wear scar. Both this and the presence of pyrophosphate was confirmed in a previous paper when examining the same tribocouples with time-of-flight mass-spectrometry.[20]

High-resolution scans of the photoelectron lines of certain elements were employed to ascertain accurate peak positions and correlate to chemical species (Table 6). Some difficulty is encountered with the S 2p and Zn 2p peak attributions as the binding energy values of the oxide and sulphide are at very similar positions. The ratio of Si to O is 1 : 1 in the worn area despite it being known that the precursor material has a Si : O ratio of 2 : 1 (Table 1). This indicates additional incorporation of O in the wear scar. As the atomic percent of O and P are 13 and 2 respectively, it can be concluded that the elevated oxygenation cannot be solely due to the formation of pyrophosphate in the wear scar.

Table 5 Nanohardness results prior to and post testing

Time point	a-C:H	Std. dev (GPa)	Si,O-DLC	Std. dev (GPa)
Unworn	22.6	6.7	15.2	4.4
14 hours	20.8	4.6	15.2	1.8

Table 6 Three spot XPS analysis of tribofilm with elements relevant to anti-wear and friction performance tabulated. Low% atomic values are due to the large contribution from carbon, which has been omitted

Si,O-DLC	Binding energy (eV)	% atomic conc.	Deviation	Attribution
Ca 2p	348.1	0.5	0.0	Calcium pyrophosphate
P 2p	133.5	1.6	0.3	Calcium pyrophosphate
S 2p	163.1	1.2	0.3	Zinc sulfide
Zn 2p	1022.1	0.2	0.1	Zinc sulfide
a-C:H	**Binding energy (eV)**	**% atomic conc.**	**Deviation**	**Attribution**
Ca 2p	346.80	0.46	0.11	Calcium carbonate
S 2p	163.4	0.52	0.36	Zinc sulfide
Zn 2p	1022.1	0.05	0.01	Zinc sulfide

TEM images of cross sections from the worn area

Bright field TEM images from FIB cross-sections of the worn areas on both samples at the end of testing are shown in Fig. 2. The Si,O-DLC coated sample shows the presence of an uneven, patchy tribofilm with a maximum thickness of 15.5 ± 1.3 nm in certain places. The a-C:H DLC sample shows a far thinner tribolayer of 2.8 ± 0.3 nm.

EELS analysis

EELS data was collected only over the DLC with care taken to avoid the tribofilms. Due to the difficult and time-consuming nature of producing cross sections of the worn area, EELS analysis was not undertaken for the 7 hour stage of the wear testing of the Si,O-doped DLC film. As discussed previously, five Gaussian peaks (labelled as G1 to G5 in Fig. 3) were fitted to the EELS carbon K-edges. An example fit from a relatively graphitic carbon material is shown in Fig. 3 (ref. 40) and the background subtracted carbon K-edge EEL spectra from the DLC films are directly compared in Fig. 4. The proportions of sp^2-bonded carbon atoms were derived from the area under the fitted peaks *via* a normalisation procedure detailed previously, these are summarised in Table 7.

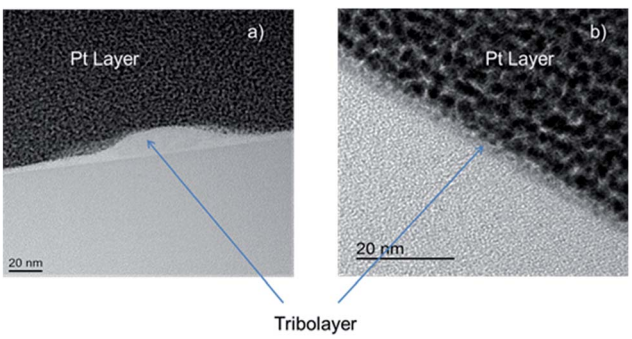

Fig. 2 Bright field TEM cross-sectional images of (a) Si,O-DLC, showing a thicker tribofilm, and (b) a-C:H DLC, showing very thin tribolayer.

Changes in carbon sp^2 fraction with wear-time

The analysis of the EELS data for the a-C:H DLC and the Si,O-DLC films at various wear times reveals an interesting trend. For both DLC films the relative proportion of planar sp^2-bonded carbon atoms remains approximately constant throughout the wear process; it being slightly higher for the a-C:H DLC film than the Si,O-DLC film, in broad agreement with the MASNMR data (Table 6). However, for the a-C:H DLC film the ratio of non-planar to planar sp^2-bonded carbon atoms increases from *ca.* 0.15 to *ca.* 0.25 (67%) – note that this analysis ignores the small contribution from C–O bonds formed during wear (Fig. 4) which might also be expected to give rise to intensity in this spectral region. This analysis implies that the newly created non-planar sp^2-hybridised carbons are derived from carbon atoms that were previously sp^3-hybridised. In contrast to planar sp^2-bonded carbon networks based on six membered rings, non-planar sp^2 bonds can be present in cyclic five- and seven-membered carbon ring systems.

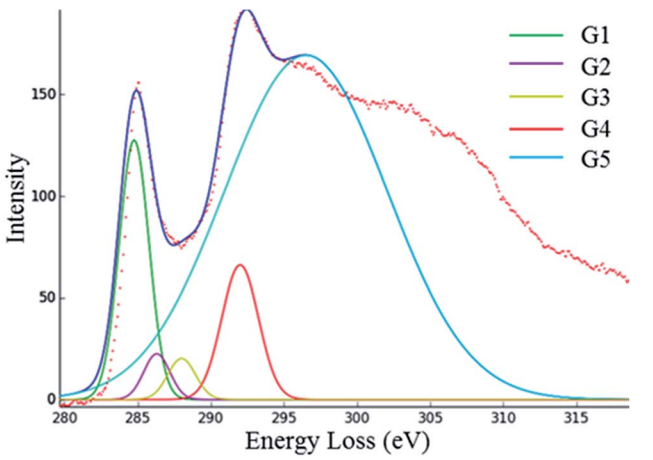

Fig. 3 Example of Hyperspy fitting of an EELS C K-edge spectrum.[40] With the first Gaussian (G1) centred at ~285 eV for the C=C π* component, G2 ~ 292 eV, the C–C σ* component and G3 ~ 300 eV, the C=C σ* component.

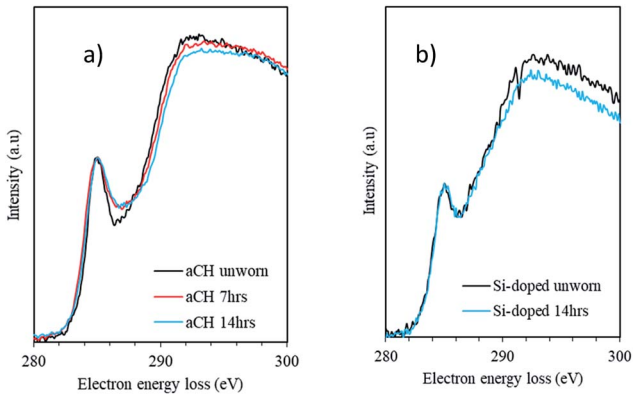

Fig. 4 Overlaid EELS spectra of (a) the a-C:H and (b) the Si,O-DLC film. The a-C:H film shows a reduction in the depth of the trough around 288 eV and is related to an increased contribution from non-planar sp^2 bonded carbon.

In comparison, no such dramatic increase in intensity in this region (G2 + G3) of the EELS carbon K-edge is observed during wear of the Si,O-doped DLC film, implying that the sp^3-hybridised carbon atoms are reasonably stable. Note that the analytical method and the extraction of non-planar sp^2-hybridised carbon atoms described in the Materials and methods section may be somewhat inappropriate for the case of these Si,O-doped DLC films owing to the significant presence of C–Si bonds and potentially C–O bonds as a result of doping (Table 1); hence the absolute values of non-planar/planar sp^2-bonded carbon atoms in Table 7 for this film may be inaccurate (denoted with an asterisk). However, the intensity in this region does not change significantly during wear and the carbon bonding in the Si,O-doped DLC film therefore remains relatively unchanged as a result of wear. In the a-C:H DLC film there is a significant reduction of sp^3-hybridised carbon atoms during wear in favour of the creation of non-planar sp^2-hybridised carbon atoms.

Discussion

Friction

Measured friction coefficients are in line with values typically associated with high-friction systems. The friction values for the two coatings are similar, with neither DLC offering greater friction reduction. This steady, high friction is to be expected, when testing in boundary lubrication with fully-formulated lubricants. When film-forming additives like ZDDP and over-based detergents are combined, they are known to form high-friction tribofilms[22,48–50] as observed here.

GMO, which has been included as friction modifier (FM), has the molecular formula $C_{21}H_{40}O_4$, and is a surfactant molecule containing a polar head group, containing both alcohol and ester moieties. These type of species are known to interact well with certain surfaces, due to the interaction of the polar head group with polar or hydroxylated surfaces.[49] GMO has been shown to be effective at reducing friction, for certain DLCs.[51] With regards to GMO and DLC, Kano *et al.*[51] note that: "The origin of low friction could be due to the very low-energy interaction between OH-terminated surfaces".[52] Si,O-DLCs are known to have many –OH terminated species.[15,20] Furthermore, the vast majority of DLCs produced by physical vapour deposition have OH-terminated surfaces; due to passivation of dangling bonds (unsaturated, carbon radicals). This happens upon exposure of the DLC coating to air, post production.[1,4] In this study it is interesting that GMO appears to offer no reduction in friction for either DLC film. The authors believe that this is due to the presence of the tribofilm that inhibits effective surface interactions between GMO and the DLCs examined in this study. Other works in the literature have identified a 'polyol–DLC interaction', this interaction would be prevented in this instance, by the formation of a tribolayer, as such layers are not rich in hydroxyl moieties.[50,53]

Coating hardness, tribofilm thickness and wear

For both coatings, the hardness values of the unworn coating when compared to the worn areas do not appear to change with wear, within experimental deviation. It may be the case that, in this instance, any tribofilm formed at the wear surface is too thin to exert an observable effect.[54] For both coatings, the experimental deviation is reduced in the worn area, most likely due to enhanced smoothing of the surfaces, so reducing error associated with the measurement.[54] ZDDP films generated on metal surfaces are typically thicker than those reported here. Such films are also seen to give different Nanohardness values than the underlying metal surface.[55] The growth of thicker tribofilms has been linked to more reactive surfaces. The trend to tribofilm thickness observed here has been noted before, in that that film thickness increases along the series: a-C:H, Si-DLC and steel.[56]

It has been proposed that thin tribofilms formed on DLCs may be related to the 'graphitization' process of amorphous

Table 7 Results of the fitting procedure applied to the EELS carbon K-edges from the DLC films. * denotes that these absolute values do not take into account intensity arising from C–Si and C–O bonds. Standard deviation is calculated from 3 the measurement areas

Sample	Mean planar sp^2%	Standard deviation	Non planar sp^2/planar sp^2	Standard deviation
a-C:H unworn	53.8%	0.5%	0.15	0.05
a-C:H 7 h	53.8%	0.5%	0.19	0.02
a-C:H 14 h	52.6%	1.3%	0.25	0.01
Si,O-Doped unworn	45.1%	2.3%	0.59*	0.07
Si,O-Doped 14 h	47.2%	1.5%	0.66*	0.04

carbon, caused by a tribochemical reaction.[57] It is hypothesised that even tribofilms of only a few nanometres in thickness can confer good levels of wear protection upon DLC surfaces.[57]

Incorporation of O within Si-doped DLCs is known to lower wear and protect the coating from thermal degradation.[31] This is due to the fact that, due to the strong thermodynamic driving force of the reaction, Si has a great propensity to react with O.[58] If Si-containing DLCs are co-doped with O, this reaction takes place as part of the formation of the tribofilm. If the Si dopant is not combined with O, the Si within the DLC will oxidise upon contact with air initiating a sequential degradation of the coating, resulting in an accelerated (oxidative) wear rate.[20,59] Furthermore, in the presence of ZDDP (well-known for its anti-oxidant ability) it would be expected that oxidation of any unreacted Si would be heavily curtailed.[20,22,60] As such, oxidative wear exacerbated by the presence of Si in the coating may be ruled out as a key wear mechanism, in this instance, allowing for a fair comparison with the a-C:H coating.

The a-C:H DLC coating was found to undergo markedly less wear than the Si,O-doped DLC. However, both coatings show clear evidence for tribofilm formation and Si,O-DLC shows a thicker tribofilm, as compared with the a-C:H coating. Although, from XPS, the Si,O-DLC tribofilm was found to contain phosphate groups, this does not seem beneficial in terms of wear suppression, despite the fact that certain phosphates containing films are well-known for their suppression of wear, *via* formation of a highly-durable layer.[22,61–64]

On steel surfaces, tribofilm thickness does not necessarily relate to lower wear.[65] When examining DLC tribopairs, the tribofilms tend to be thinner as compared with those formed on steel surface.[66] The difference in tribofilm thickness between the Si,O-DLC and a-C:H DLC coatings suggests that the wear is independent of thickness and doping the DLC coating with Si makes the DLC coating more "ferrous-like", in that it behaves more like a steel surface. This behaviour has been noted previously for DLCs with more reactive surfaces, allowing thicker tribofilms.[56] This suggests that several mechanisms are governing the overall wear rate and further underlines the complexities of wear mechanisms and predictions within oil lubricated steel/DLC contacts.[67]

Tribofilm structure and chemistry

XPS analysis confirmed the presence of tribofilms (containing Ca, Zn and S) on both DLC coatings, after 14 hours of wearing. Ca-rich tribofilms are to be expected when ZDDP is combined with Ca over-based detergents, as Ca^{2+} cations can compete with Zn^{2+} for incorporation within the phosphate network.[25,68]

XPS also confirmed the presence of P in the tribofilm on the Si,O-doped sample, whereas none was detected on the a-C:H sample. In previous work on the same system, P has been confirmed as being present as phosphate-type species, by ToF-SIMS analysis.[20] Polyphosphates are known to play an important role with regards to wear suppression, due to their ability to form a hard, wear resistant film.[22] However, the presence of polyphosphate chains were not noted in this instance and instead calcium phosphate was detected in the tribofilm on the Si,O-DLC. Polyphosphate chains were not detected in these samples.

The presence of calcium phosphate on the Si,O-DLC suggests that the coating is more similar to a ferrous surface than a non-doped DLC. This behaviour can be rationalized by the fact that doping the DLC with Si increases water wettability, due to the presence of polar Si–O groups at the surface of the coating.[17] This behaviour is not paralleled with the tribofilm formed on the (less polar) a-C:H DLC where calcium carbonate was identified by XPS. This species has been shown to exhibit good anti-wear properties.[27,69] Not only is calcium carbonate detected on the a-C:H DLC tested here, its formation at steel-DLC contacts has also been identified in other studies.[68] This key difference in tribofilm chemistry is contributing to the differing wear behaviour of the two coatings.

NMR and EELS analysis

We have employed two distinct methods for ascertaining carbon hybridisation states. Some differences between the two analytical techniques are to be expected, as they have different mechanisms for establishing carbon hybridisation state and are vulnerable to different data acquisition artefacts, as discussed previously.[9] However, analysis of both the MASNMR and EELS data indicated that the level of (planar) sp^2-bonded carbon in the a-C:H DLC coating was higher than that in the Si,O-doped DLC coating. Analysis of the EELS carbon K-edge was used to extract the non-planar sp^2-bonded carbon signal, however potentially this species may contribute to the MASNMR signal for sp^2-bonded carbon.

For the a-C:H DLC coating, summing the planar and non-planar sp^2-bonded carbon contributions from the EELS data and correcting for the proportion of C–O bonds present (from NMR data in Table 3) gives an almost identical value for the total carbon sp^2 fraction in the film to that derived from ^{13}C MASNMR. The same comparison for the Si,O-doped DLC coating is complicated by the presence of C–Si bonding, however we note that the planar sp^2 carbon fraction is similar to that derived from NMR. This agreement would appear to confirm the carbon sp^2 values presented herein, suggesting that the Si,O-doped DLC has a higher amount of sp^3 bonding than the a-C:H DLC.

Changes in carbon bonding with wear

Changes in carbon hybridisation state within the a-C:H DLC film as a function of testing time were observed by EELS. This time dependence appears to arise from either the wear processes, or perhaps also the heat generated by tribotesting. The re-hybridisation seen within the a-C:H DLC coating suggested that sp^3-bonded carbon atoms transformed to non-planar sp^2 bonded carbon atoms. Whilst the proportion of planar sp^2 hybridised carbon atoms remained relatively constant, the ratio of non-planar to planar sp^2 hybridised carbon atoms increased from 0.15 to 0.25 over a 14 hour period; corresponding to a 67% increase. Conversely, there was not such a large change observed for the Si,O-doped DLC coating. Changes in sp^2 ratios of DLC coatings with heating have been

previously reported in the literature, and could be a contributing factor here.[2,3]

From EELS data, it appears that the formations of non 6-membered carbon rings are the most likely candidates for the increase in non-planar sp^2 bonding within the within the a-C:H DLC during wear. These species are reported in the literature for fullerenes, carbon nanotubes and graphene, all of which share some similarities with DLC.[70–73]

The conversion of sp^3 carbon bonds to non-planar sp^2 carbon bonds seems to be correlated with the lower wear of the a-C:H DLC coating, when compared with the Si,O-doped DLC. This is in addition to the wear suppression provided by the differing tribofilm chemistries. It appears to be the case that the conversion of sp^3 to non-planar sp^2 bonds is thermodynamically favourable under the tribological conditions examined; specifically the increased pressure and temperature at the contact.

Although the authors do not observe graphitisation *per se* of either DLC coating as a result of wear, it is believed that a crucial step in the conversion of the a-C:H DLC to a more stable material has been identified. This being the aforementioned conversion of carbon sp^3 bonds to non-planar sp^2 bonds, which could be analogous to the very early steps of graphitisation of the DLC. In normal graphitising carbons, such effects are seen at around 800 °C when under atmospheric pressure.[74] The conversion is apparent when the carbon K-edge EELS spectra for the a-C:H DLC pre- and post-wear is overlaid, as shown in Fig. 4. The authors note that thermal treatment of DLC coatings has been linked to the re-hybridization of carbon bonding within the coating. However, typically this change takes place at far higher temperatures (in excess of 400 °C) than those encountered in these tests.[2]

The Si,O-doped DLC coating appears to be more stable with regards to carbon hybridisation during wear. This resistance to rehybridisation is most likely due to the inability of Si to form stable double bonds; thus forcing it to bond in a sp^3 fashion within the coating and therefore securing a network of carbon atoms in this configuration.[45]

Conclusions

A variety of analytical techniques have been used to fully characterize the tribochemical performance of the two DLC coatings: an a-C:H DLC coating and a Si,O-doped DLC coating. The two coatings exhibited distinctly different behaviours in terms of wear, tribofilm formation, tribofilm thickness, and changes carbon hybridisation-state during wear.

The key findings within this work were:

• The two DLC coatings exhibited very similar coefficients of friction when lubricated in fully-formulated engine oil;

• At 14 hours of testing, the Si,O-doped DLC coating had a thicker tribofilm than the a-C:H DLC coating. This enhanced tribofilm thickness did not appear to facilitate lower wear rates;

• The two coatings had Nanohardness values within experimental deviation of each other, confirming that hardness did not play a crucial role in wear;

• The tribofilms on the two coatings exhibited notable differences with respect to phosphorous content. This is noteworthy as certain phosphorous films are well-known for their ability to repress wear;

• The phosphorous species formed on the Si,O-doped DLC coating did not facilitate lower wear as effectively as the calcium carbonate species observed on the a-C:H DLC;

• EELS identified a clear difference in performance between the two DLC coatings tested. This appeared to be related to an increase in the non-planar carbon sp^2 fraction within the a-C:H DLC during wear. This increase was derived from previously sp^3 bonded carbons. The Si,O-DLC coating is stable in regards to its carbon sp^2 and sp^3 content.

We have proposed a dual mechanism for the lower wear of the a-C:H DLC coating involving both re-hybridisation of carbon bonding within the a-C:H coating and the formation of different Ca-containing protective tribofilms. The incorporation of Si within the Si,O-doped DLC hinders any transformation in carbon hybridisation state within the DLC. We believe that, in this instance, this is a key contributor to the higher wear rate observed in the Si-doped DLC. This result may appear unexpected as, in terms of wear of DLCs, sp^3 type bonding is often regarded as superior and more 'diamond-like'. We propose that inherent resistance to microstructural changes within DLC coatings are detrimental with regards to the wear performance of the coating.

Conflicts of interest

In accordance with RSC's policy on Conflicts of interest, there are no conflicts to declare.

Acknowledgements

X-ray photoelectron spectra were obtained at the National EPSRC XPS Users' Service (NEXUS) at Newcastle University, an EPSRC Mid-Range Facility. Solid-state NMR spectra were obtained at the EPSRC UK National Solid-state NMR Service at Durham.

References

1 Y. Yamauchi, M. Kuzuya, Y. Sasai and S. Kondo, *Thin Solid Films*, 2011, **519**, 6693–6697.
2 R. Kalish, Y. Lifshitz, K. Nugent and S. Prawer, *Appl. Phys. Lett.*, 1999, **74**, 2936–2938.
3 D. S. Grierson, A. V. Sumant, A. R. Konicek, T. A. Friedmann, J. P. Sullivan and R. W. Carpick, *J. Appl. Phys.*, 2010, **107**, 033523.
4 Y. Yamauchi, Y. Sasai, S.-I. Kondo and M. Kuzuya, *Thin Solid Films*, 2010, **518**, 3492–3496.
5 A. A. Voevodin and J. S. Zabinski, *Diamond Relat. Mater.*, 1998, **7**, 463–467.
6 M. Veres, M. Koós, S. Tóth, M. Füle, I. Pócsik, A. Tóth, M. Mohai and I. Bertóti, *Diamond Relat. Mater.*, 2005, **14**(3–7), 1051–1056.

7 R. A. Wolkow and M. Moskovits, *J. Chem. Phys.*, 1992, **96**, 3966–3980.
8 J. Schwan, S. Ulrich, V. Batori, H. Ehrhardt and S. R. P. Silva, *J. Appl. Phys.*, 1996, **80**, 440–447.
9 T. Iseki, H. Mori, H. Hasegawa, H. Tachikawa and K. Nakanishi, *Diamond Relat. Mater.*, 2006, **15**(4–8), 1004–1010.
10 L. Ponsonnet, C. Donnet, K. Varlot, J. M. Martin, A. Grill and V. Patel, *Thin Solid Films*, 1998, **319**, 97–100.
11 J. C. Damasceno, S. S. Camargo Jr, F. L. Freire Jr and R. Carius, *Surf. Coat. Technol.*, 2000, **133–134**, 247–252.
12 R. West, M. J. Fink and J. Michl, *Science*, 1981, **214**, 1343–1344.
13 R. Gilmore and R. Hauert, *Thin Solid Films*, 2001, **398–399**, 199–204.
14 M.-G. Kim, K.-R. Lee and K. Y. Eun, *Surf. Coat. Technol.*, 1999, **112**, 204–209.
15 K. Oguri and T. Arai, *J. Mater. Res.*, 2011, **7**, 1313–1316.
16 D.-C. Pham, H.-S. Ahn, J.-E. Oh and E.-S. Yoon, *J. Mech. Sci. Technol.*, 2007, **21**, 1083–1089.
17 M. Grischke, A. Hieke, F. Morgenweck and H. Dimigen, *Diamond Relat. Mater.*, 1998, **7**, 454–458.
18 J. Ando, T. Ohmori, A. Murase, N. Takahashi, T. Yamaguchi and K. Hokkirigawa, *Wear*, 2009, **266**, 239–247.
19 M. Ban, M. Ryoji, S. Fujii and J. Fujioka, *Wear*, 2002, **253**, 331–338.
20 J. Lanigan, H. Zhao, A. Morina and A. Neville, *Tribol. Int.*, 2015, **82**, 431–442.
21 S. Kosarieh, A. Morina, E. Lainé, J. Flemming and A. Neville, *Wear*, 2013, **302**, 890–898.
22 H. Spikes, *Tribol. Lett.*, 2004, **17**, 469–489.
23 N. J. Mosey, M. H. Müser and T. K. Woo, *Science*, 2005, **307**, 1612–1615.
24 M. Shiomi, M. Tokashiki, H. Tomizawa and T. Kuribayashi, *Lubr. Sci.*, 1989, **1**, 131–147.
25 Y. Wan, M. L. Suominen Fuller, M. Kasrai, G. M. Bancroft, K. Fyfe, J. R. Torkelson, Y. F. Hu and K. H. Tan, in *Tribology Series*, ed. M. P. G. D. D. Dowson and A. A. Lubrecht, Elsevier, 2002, vol. 40, pp. 155–166.
26 M. Kasrai, M. S. Fuller, G. M. Bancroft and P. R. Ryason, *Tribol. Trans.*, 2003, **46**, 534–542.
27 M. Najman, M. Kasrai, G. Michael Bancroft and R. Davidson, *Tribol. Int.*, 2006, **39**, 342–355.
28 W. C. Oliver and G. M. Pharr, *J. Mater. Res.*, 1992, **7**, 1564–1583.
29 A. Albertazzi, M. R. Viotti, R. M. Miggiorin and A. Dal Pont, in *Interferometry XIV: Applications*, ed. E. L. Novak, W. Osten and C. Gorecki, Spie-Int Soc Optical Engineering, Bellingham, 2008, vol. 7064.
30 H. Liu and T. J. Webster, *Biomaterials*, 2007, **28**, 354–369.
31 W.-J. Wu and M.-H. Hon, *Surf. Coat. Technol.*, 1999, **111**, 134–140.
32 G. B. D. Briggs, *High Resolution XPS of Organic Polymers*, Wiley, Chichester, 1992.
33 D. Briggs, *Surface analysis of Polymers by XPS and static SIMS*, OUP, Cambridge, 1998.
34 J. Moulder, W. Stickle and P. Sobol, *Handbook of X Ray Photoelectron Spectroscopy (P/N 624755)*, Perkin-Elmer, Physical Electronics Division, 1992.
35 M. R. Alexander, R. D. Short, F. R. Jones, W. Michaeli and C. J. Blomfield, *Appl. Surf. Sci.*, 1999, **137**, 179–183.
36 R. F. Egerton, P. Li and M. Malac, *Micron*, 2004, **35**, 399–409.
37 J. P. McCaffrey, M. W. Phaneuf and L. D. Madsen, *Ultramicroscopy*, 2001, **87**, 97–104.
38 J. Fontaine, C. Donnet, A. Grill and T. LeMogne, *Surf. Coat. Technol.*, 2001, **146–147**, 286–291.
39 C. Donnet, J. Fontaine, A. Grill and T. Le Mogne, *Tribol. Lett.*, 2001, **9**, 137–142.
40 B. E. Mironov, H. M. Freeman, A. P. Brown, F. S. Hage, A. J. Scott, A. V. K. Westwood, J. P. Da Costa, P. Weisbecker and R. M. D. Brydson, *Carbon*, 2015, **83**, 106–117.
41 B. Mironov, H. Freeman, A. Brown, F. Hage, A. Scott, A. Westwood, J.-P. Da Costa, P. Weisbecker and R. Brydson, *Carbon*, 2015, **83**, 106–117.
42 A. LiBassi, A. C. Ferrari, V. Stolojan, B. K. Tanner, J. Robertson and L. M. Brown, *Diamond Relat. Mater.*, 2000, **9**, 771–776.
43 D. Shindo, T. Musashi, Y. Ikematsu, Y. Murakami, N. Nakamura and H. Chiba, *J. Electron Microsc.*, 2005, **54**, 11–17.
44 P. Papakonstantinou, J. F. Zhao, P. Lemoine, E. T. McAdams and J. A. McLaughlin, *Diamond Relat. Mater.*, 2002, **11**, 1074–1080.
45 Y. Wang, Y. Xie, P. Wei, R. B. King, H. F. Schaefer, P. v. R. Schleyer and G. H. Robinson, *Science*, 2008, **321**, 1069–1071.
46 T. Yamaguchi, J. Ando, T. Tsuda, N. Takahashi, M. Tohyama, A. Murase, T. Ohmori and K. Hokkirigawa, *Tribol. Int.*, 2011, **44**, 1296–1303.
47 C. C. Chusuei, D. W. Goodman, M. J. Van Stipdonk, D. R. Justes and E. A. Schweikert, *Anal. Chem.*, 1999, **71**, 149–153.
48 L. J. Taylor and H. A. Spikes, *Tribol. Trans.*, 2003, **46**, 303–309.
49 K. Topolovec-Miklozic, T. R. Forbus and H. Spikes, *Tribol. Lett.*, 2008, **29**, 33–44.
50 K. Topolovec-Miklozic, F. Lockwood and H. Spikes, *Wear*, 2008, **265**, 1893–1901.
51 M. Kano, Y. Yasuda, Y. Okamoto, Y. Mabuchi, T. Hamada, T. Ueno, J. Ye, S. Konishi, S. Takeshima, J. M. Martin, M. I. De Barros Bouchet and T. L. Mognee, *Tribol. Lett.*, 2005, **18**, 245–251.
52 M. Kano, Y. Yasuda, Y. Okamoto, Y. Mabuchi, T. Hamada, T. Ueno, J. Ye, S. Konishi, S. Takeshima, J. M. Martin, M. I. D. Bouchet and T. Le Mogne, *Tribol. Lett.*, 2005, **18**, 245–251.
53 M. Kano, *New Diamond Front. Carbon Technol.*, 2006, **16**, 201–210.
54 W.-G. Jiang, J.-J. Su and X.-Q. Feng, *Eng. Fract. Mech.*, 2008, **75**, 4965–4972.
55 N. N. Gosvami, J. A. Bares, F. Mangolini, A. R. Konicek, D. G. Yablon and R. W. Carpick, *Science*, 2015, **348**, 102–106.
56 M. Kalin, E. Oblak and S. Akbari, *Tribol. Int.*, 2016, **96**, 43–56.

57 H. S. Ahn, S. A. Chizhik, A. M. Dubravin, V. P. Kazachenko and V. V. Popov, *Wear*, 2001, **249**, 617–625.
58 P. A. Rock, *Chemical Thermodynamics*, University Science Books, Science, 19 Jun 2013, p. 548, https://books.google.cz/books/about/Chemical_Thermodynamics.html?id=TLJoF9kizrAC&redir_esc=y.
59 J. L. Lanigan, C. Wang, A. Morina and A. Neville, *Tribol. Int.*, 2016, **93**, 651–659.
60 B. Liu and V. Gatto, in *Proceedings of the FISITA 2012 World Automotive Congress: Volume 1: Advanced Internal Combustion Engines (I)*, Springer Berlin Heidelberg, Berlin, Heidelberg, 2013, pp. 559–569, DOI: 10.1007/978-3-642-33841-0_43.
61 G. Pereira, A. Lachenwitzer, M. A. Nicholls, M. Kasrai, P. R. Norton and G. D. Stasio, *Tribol. Lett.*, 2005, **18**, 411–427.
62 J. Martin, *Tribol. Lett.*, 1999, **6**, 1–8.
63 M. Aktary, M. T. McDermott and G. A. McAlpine, *Tribol. Lett.*, 2002, **12**, 155–162.
64 R. K. Brow, D. R. Tallant, S. T. Myers and C. C. Phifer, *J. Non-Cryst. Solids*, 1995, **191**, 45–55.
65 Z. Zhang, E. S. Yamaguchi, M. Kasrai and G. M. Bancroft, *Tribol. Lett.*, 2005, **19**, 211–220.
66 S. Equey, S. Roos, U. Mueller, R. Hauert, N. D. Spencer and R. Crockett, *Tribol. Int.*, 2008, **41**, 1090–1096.
67 Z. Lu, L. Wang, G. Zhang and Q. Xue, *Tribol. Lett.*, 2011, **41**, 435–438.
68 T. Kubo, S. Fujiwara, H. Nanao, I. Minami and S. Mori, *Wear*, 2008, **265**, 461–467.
69 M. Zhang, X. Wang, X. Fu and Y. Xia, *Tribol. Int.*, 2009, **42**, 1029–1039.
70 Y.-Z. Tan, R.-T. Chen, Z.-J. Liao, J. Li, F. Zhu, X. Lu, S.-Y. Xie, J. Li, R.-B. Huang and L.-S. Zheng, *Nat. Commun.*, 2011, **2**, 420.
71 Z. L. Wang and Z. C. Kang, *J. Phys. Chem.*, 1996, **100**, 17725–17731.
72 A. Hashimoto, K. Suenaga, A. Gloter, K. Urita and S. Iijima, *Nature*, 2004, **430**, 870–873.
73 S. lijima, T. Ichihashi and Y. Ando, *Nature*, 1992, **356**, 776–778.
74 H. Daniels, R. Brydson, B. Rand and A. Brown, *Philos. Mag.*, 2007, **87**, 4073–4092.